remote sensing

MDPI

Article

Classifying Sparse Vegetation in a Proglacial Valley Using UAV Imagery and Random Forest Algorithm

Ulrich Zangerl *, Stefan Haselberger and Sabine Kraushaar

Department of Geography and Regional Research, University of Vienna, Universitätsstraße 7, 1010 Vienna, Austria

* Correspondence: ulrich.zangerl@univie.ac.at

Abstract: Extreme hydro-meteorological events become an increasing risk in high mountain environments, resulting in erosion events that endanger human infrastructure and life. Vegetation is known to be an important stabilizing factor; however, little is known about the spatial patterns of species composition in glacial forelands. This investigation aims to differentiate sparse vegetation in a steep alpine environment in the Austrian part of the Central Eastern Alps using low-cost multispectral cameras on an unmanned aerial vehicle (UAV). Highly resolved imagery from a consumer-grade UAV proved an appropriate basis for the SfM-based modeling of the research area as well as for vegetation mapping. Consideration must be paid to changing light conditions during data acquisition, especially with multispectral sensors. Different approaches were tested, and the best results were obtained using the Random Forest (RF) algorithm with the target class discrimination based on the RGB orthomosaic and the DEM as supplementary dataset. Our work contributes to the field of biogeomorphic research in proglacial areas as well as to the field of small-scale remote sensing and vegetation measuring. Our findings show that the occurrence of vegetation patches differs in terms of density and diversity within this relatively recent deglaciated environment.

Keywords: UAV remote sensing; vegetation mapping; structure from motion

Citation: Zangerl, U.; Haselberger, S.; Kraushaar, S. Classifying Sparse Vegetation in a Proglacial Valley Using UAV Imagery and Random Forest Algorithm. *Remote Sens.* **2022**, *14*, 4919. https://doi.org/10.3390/rs14194919

Academic Editor: Javier J Cancela

Received: 16 June 2022
Accepted: 30 August 2022
Published: 1 October 2022

1. Introduction

Erosion processes, such as landslides, debris flows or rockfalls, constitute a permanent threat to human settlements and infrastructure in high mountain environments [1]. Vegetation cover can stabilize affected slopes and reduce the amount of eroded material [2]. Hence, the establishment of vegetation cover is of great interest to local communities. In an area of fast glacial retreat, primary succession begins from zero with the establishment of pioneer species [3–5]. In the following years, different species try to settle, and the local ecosystem becomes denser and more diverse. The earlier this colonization occurs, the better erosion can be counteracted. Geoecological succession, however, is not a simple one-way sequence of development stages, and successional pathways are not always this straight [5]. Increasing vegetation cover goes along with the development of soils, and if enough sediment is stabilized, the intensity of geomorphological activities decreases [6]. Disturbances may still occur and hamper the progress of the successional development resulting in a diverse spatial pattern of different successional stages along the area of glacial retreat.

Robust approaches for vegetation estimation using satellite data such as Sentinel or Landsat in combination with vegetation indices have been developed in recent years [7,8], and especially the Sentinel series is still widely used for scientific research [9], but even with state-of-the-art sensor technology, there remains the problem of the insufficient spatial resolution of satellite-based data for various applications such as the detection and discrimination of small plants. Unmanned aerial systems have experienced a massive upswing in usage in the last decade and are partially able to close the gap between the fast-but-coarse satellite sensing technologies and time-intensive data collection directly in the field. In

conventional remote sensing approaches, the collection of field observations for training- and reference data was a time-consuming process that was also connected with further obstacles such as geolocation inaccuracies and biases. In very high resolution (VHR-) datasets, samples are extracted directly from the images since the visual identification of the target classes is possible in highly resolved imagery [10]. Using data from UAVs for vegetation classification has several advantages, such as the provision of three-dimensional information through the Structure from Motion (SfM) technology, as well as the use of low-cost multispectral sensors [11–15]. The upscaling of fundamental biogeomorphical research is facilitated by high-resolution vegetation data of the study area.

Key research questions here are:

1. What are the limitations of low-cost multispectral cameras fixed on commercially available UAVs in the context of vegetation remote sensing in proglacial areas?
2. What combination of input parameters (e.g. sensors and Terrain Ruggedness Index) delivers the best accuracy results with regard to land cover?
3. What spatial resolution could be achieved in terms of the vegetation cover classification in the glacial foreland?

2. Materials and Methods

2.1. Study Area

The Kaunertal valley is located in western Austria (federal state Tyrol) and is situated in the Ötztaler Alps, which are part of the crystalline Central Eastern Alps. The Gepatschferner glacier at the southern end of the valley is the second largest glacier in Austria. The study area is a hanging side-valley west of the retreating Gepatschferner glacier tongue and comprises roughly 1.75 km^2 in size. Altitudes range from 2300 to 2900 m above sea level. The bedrock consists of more than 70% paragneiss, in combination with orthogneisses and amphibolites [16,17]. The present climate is characterized by a relatively low amount of precipitation and low temperatures throughout the whole year, classifying the Kaunertal as an inner-alpine dry valley [17,18]. The once glaciated catchment shows a distinctive U Shape with lateral, middle and end moraine features, as well as various roche moutonnées along the perennial river, which in parts is a braided river system of Strahler stream order one. The steep alpine slopes and the relatively young (<170 years) deglaciated unconsolidated moraine sediments are prerequisites for high geomorphological activity. Rockfalls, debris flows and some landslides can be observed throughout the study area [17]. The research area is only sparsely vegetated. Due to the lack of sunshine, long-lasting snow cover and high geomorphologic activity, the highest growing plants are Juniperus and Salixes, with a maximum height of 50 cm. Different terrain ages can be observed along the area of glacier retreat, interrupted by patches of geomorphic activity or stability (see Figure 1). The area in the south-west has been ice-free for roughly 50 years, so an intermediate successional stage would be expected here. Bordering it on the lower side, areas of higher terrain age are located, which have been ice-free for approximately 100 years and fall into the late successional stage [5]. The former extent of the Little Ice Age (≈170 years ago) is clearly visible below in the form of distinct moraines.

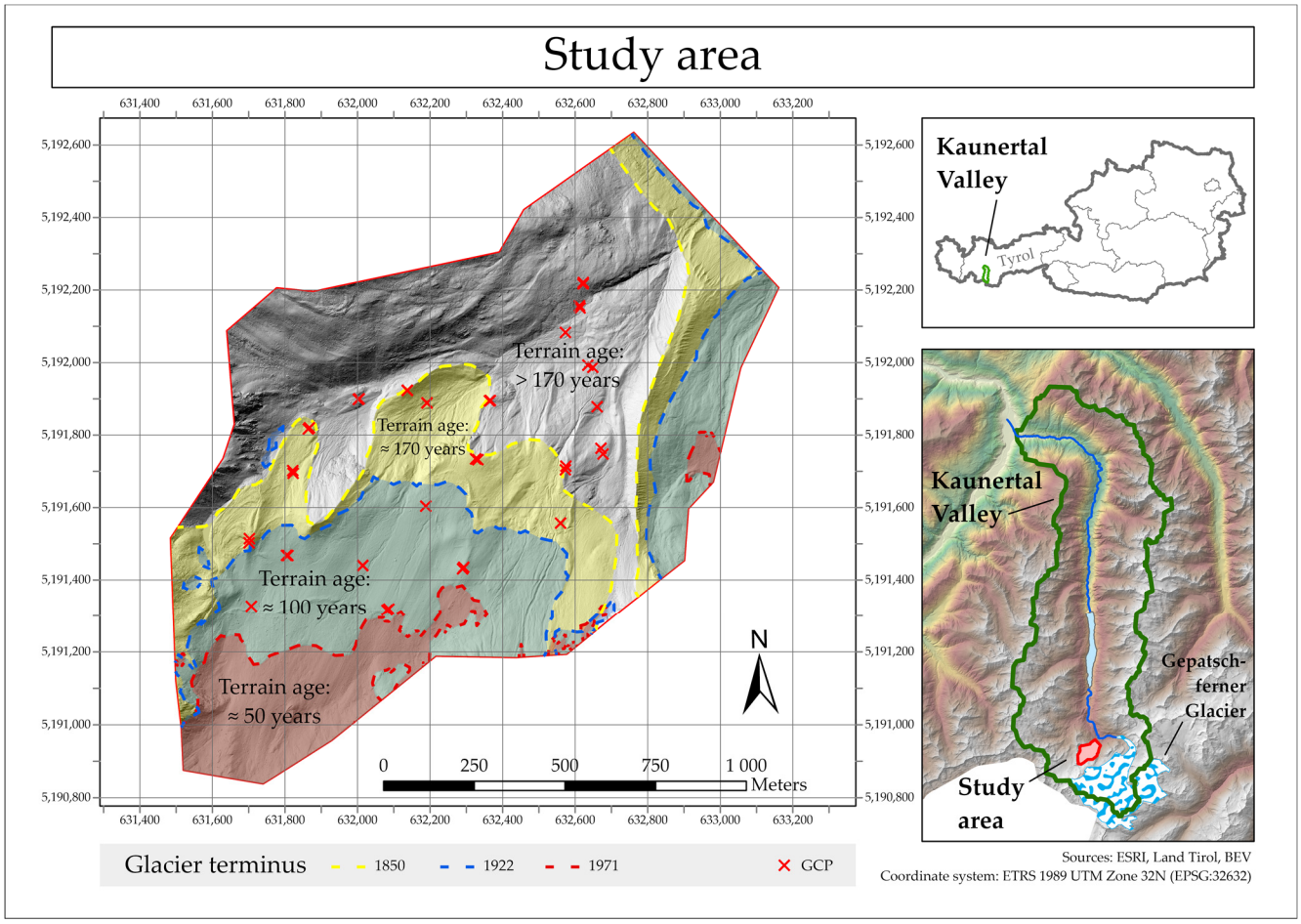

Figure 1. Study area. Overview and detailed map of the study area with glacier terminus lines and successional stages. The study area is located in the federal state of Tyrol in Austria.

2.2. Data Collection

The data collection took place at the beginning of August 2019 over the course of three days. In total, 39 ground control points (GCPs) were arranged in the study area, some of which were sprayed on rocks and some fixed on the ground as laminated A3 printouts. The GCPs were located using a Trimble Zephyr 3 differential GNSS receiver.

A DJI Phantom 4 Pro V2.0 equipped with a 1-inch 20-megapixel CMOS sensor and a focal length of 8.8 mm/24 mm (35 mm equivalent) [19] and two mounted multispectral cameras from MAPIR (https://www.mapir.camera/ (accessed on 10 January 2022)) was used to obtain high-resolution imagery of the research area. One camera captured images in the red edge (RE) channel (725 nm), which acted as an indicator of plant productivity by measuring the chlorophyll content in leaves [20,21]. The second camera employed a combination of three spectral bands (OCN; orange: 490 nm, cyan: 615 nm, near-infrared: 808 nm), which were used to measure sparse vegetation on bare soil or in between rocks [22]. Both cameras used a 12-megapixel Sony Exmor R IMX117 sensor with a focal length of 19 mm and produced images with 4000 × 3000 pixels [23]. These cameras were originally designed for agricultural use, but due to the relatively low cost and promising spectral variety, we decided to use them as a supplement in our research approach. We used the flight planning application drone harmony (https://droneharmony.com/ (accessed on 1 June 2022)) to create four tailored flight plans of the study area with a front overlap of 80 percent and a side overlap of 70 percent while taking nadir pictures. These flight plans were designed as terrain-aware, which means that the UAV kept a constant height of 60 m above the underlying ground. The imagery has an average ground sampling distance (GSD) of 1.85 cm/pixel

for the onboard RGB camera and a GSD of 2.25 cm/pixel for the multispectral cameras. Due to time and resource constraints, all three sensors were attached to the UAV simultaneously. In order to counteract exposure fluctuations, the flights were attempted to be carried out under constant light conditions, which was only partially possible due to the weather situation and the alpine terrain, which cast large shadows. Furthermore, the calibration target provided by MAPIR was used.

2.3. Data Processing

Data processing was undertaken separately for the RGB imagery and the multispectral imagery. The multispectral pictures needed to be preprocessed and calibrated in the software application MAPIR Camera Control, turning the recorded pixel values into reflection values for the respective bands. Then, the captured RAW and JPEG images were combined with TIFF images.

The photogrammetric processing procedure (SfM) in Agisoft Metashape (https://www.agisoft.com/ (accessed on 3 May 2022)) followed the workflow described by the United States Geological Survey [24] and was modified in line with on-site experience. The modifications included removing the camera positions before the alignment process to minimize matching issues, using filtering options customized to the data, and building the orthomosaic on the basis of the DEM, which is reliable for aerial surveys. The workflow was carried out using high settings in the Agisoft dialogues with the same configurations for each set of images. Adaptive camera model fitting was activated, and low-quality pictures were removed beforehand. Image quality was assessed inside Agisoft with a drop-out threshold of <0.5. The project was rectified and georeferenced using 39 ground control points, of which nine were used as check points for uncertainty estimation. Table 1 shows the uncertainty values (RMSE) for the control points and check points:

Table 1. Uncertainty values: The RMSE for the control points and check points.

	Count	X Error (cm)	Y Error (cm)	Z Error (cm)	XY Error (cm)	Total (cm)
Control points	30	3.20	3.27	5.44	4.58	7.11
Check points	9	3.66	4.37	5.53	5.70	7.94

The derived products from the photogrammetric processing in Agisoft were:

- Digital elevation model (from RGB imagery, spatial resolution: 10 cm/pixel);
- True color orthomosaic (from RGB imagery, spatial resolution: 4.5 cm/pixel);
- False color orthomosaic (from OCN imagery, spatial resolution: 4.5 cm/pixel);
- False color orthomosaic (from RE imagery, spatial resolution: 4.5 cm/pixel).

Changing weather conditions led to variations in the illumination of the recorded pictures and to inconsistent brightness values across the final orthomosaic. This caused difficulties in the further course of the classification procedure.

Machine Learning Methods

Different machine learning (ML) methods, including Convolutional Neural Networks (CNNs) and RF, were tested in this work. Tests using the CNNs did not deliver promising results and overstrained our computational capacities and were therefore dismissed. An RF machine learning algorithm was chosen to classify the vegetation based on the orthomosaics because of its robust and reliable functionality. RF has proven very successful for comparable applications in the field of land cover classification and vegetation mapping [25–28]. The RF classifier makes predictions based on a set of classification and regression trees (CARTs) and is insensitive to overfitting and robust when handling inconsistencies in spectral response [29–32]

Class balance and a high target representation were ensured by skilled personnel manually selecting samples directly from the highly resolved orthomosaic. To warrant

independent validation data, 20% of the samples were excluded from the training process and used for validation after the classification process. These samples were chosen randomly from the entirety of the samples to avoid any kind of bias. In total, 3345 samples were digitized by hand, from which 2686 were used for training and 659 for validation. The results of the validation process are presented in Table 2.

Table 2. Land cover classes and number of ground truthing samples used for the classification.

Class Value	Class Description	Number of Samples
1	Snow	423
2	Water	307
3	Bedrock	399
4	Coarse sediment	585
5	Fine sediment	305
6	Juniper (*Juniperus communis*)	300
7	Thistle (*Cirsium spinosissimum)*	399
8	Mixed vegetation with >50% grass	310
9	Mixed vegetation with >50% forbs and moss	317

We distinguished between nine land cover classes that were defined as follows:

Normally, the RF classifier is able to detect the variables which are most suitable for differentiating the predefined target classes, but for this paper, this step was performed by hand. This was because the RF tool implemented in ArcGIS Pro does not offer this functionality due to the low number of available variables.

Training and classification were carried out with the implemented RF algorithm in ArcGIS Pro. RF achieves higher accuracy values when more trees are used, but this also increases the computational resources required [31]. Different studies, however, show that constantly increasing the number of trees does not necessarily lead to better model performance. Above a certain number of trees, no significant improvements were detectable [33,34]. We used 50 trees and a tree depth of also 50 as a starting point for figuring out the appropriate values for our application. Then the classification procedure was performed multiple times under consistent initial conditions except for the number of trees and the tree depth, respectively, which were adjusted for each test run. For our final classification, we used 100 trees and a tree depth of also 100 because with these values, the best classification results were obtained. Tests using a higher number for these values did not significantly improve the outcome. Except for the parameters we assessed ourselves, we followed the manufacturer's [35] recommendations, e.g., regarding the maximum number of samples per class that can be used, which is 1000 samples for unsegmented rasters. The training and classification processes were based on the RGB orthomosaic from which the samples were taken, utilizing the digital elevation model as an ancillary input dataset. Other supplementary datasets such as the OCN orthomosaic, the RE orthomosaic, the Terrain Ruggedness Index (TRI) and a slope layer were tested as well by adding them to the classification process instead of the DEM. The reached accuracy values for each layer are presented in the results section.

3. Results

In the OCN and RE orthomosaics (Figures 2 and 3), changing illumination conditions during the survey are visible and could not be eliminated using the MAPIR calibration target. Fluctuations in brightness influenced the reflection values of the multispectral imagery more strongly than the actual variance in vegetation on the ground. The integrated vibration dampers did not meet the requirements of our application. Camera instabilities resulted in partly blurry images even when paying attention to the camera settings (shutter speed, ISO value). Faulty reflection values (Figure 2) occurred randomly and could not be traced to certain cover changes. Geometrical artifacts looking somewhat

like rocks appeared in the digital elevation model during photogrammetric processing (see Supplementary Materials).

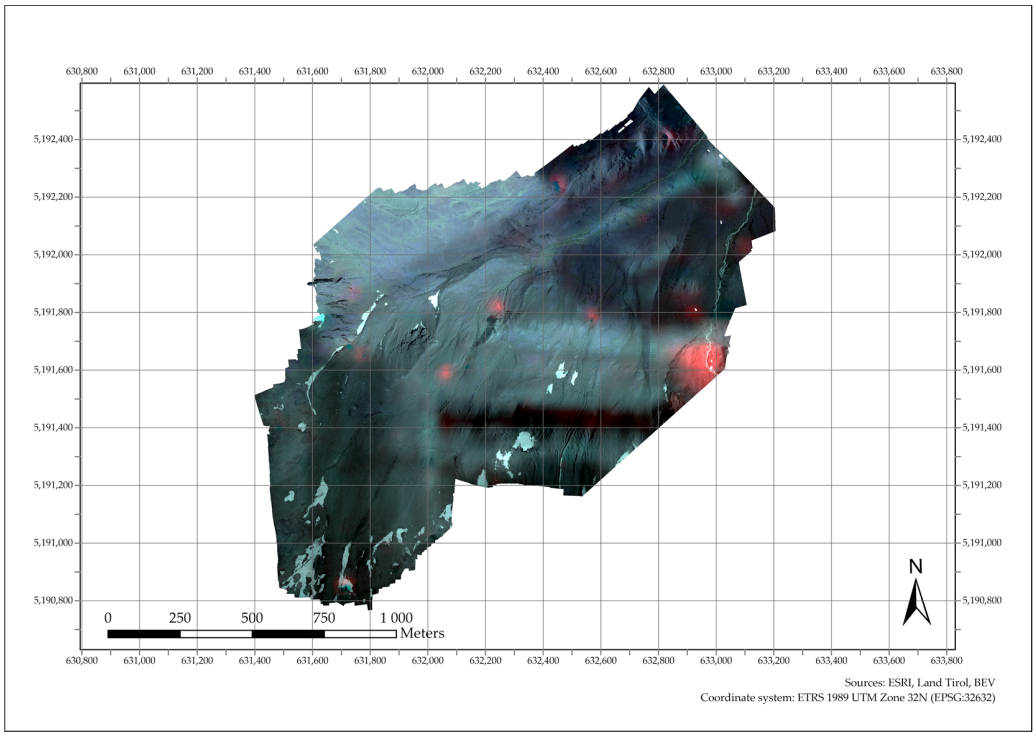

Figure 2. The OCN orthomosaic with different illumination conditions. Red areas are interpreted as artifacts due to illumination conditions.

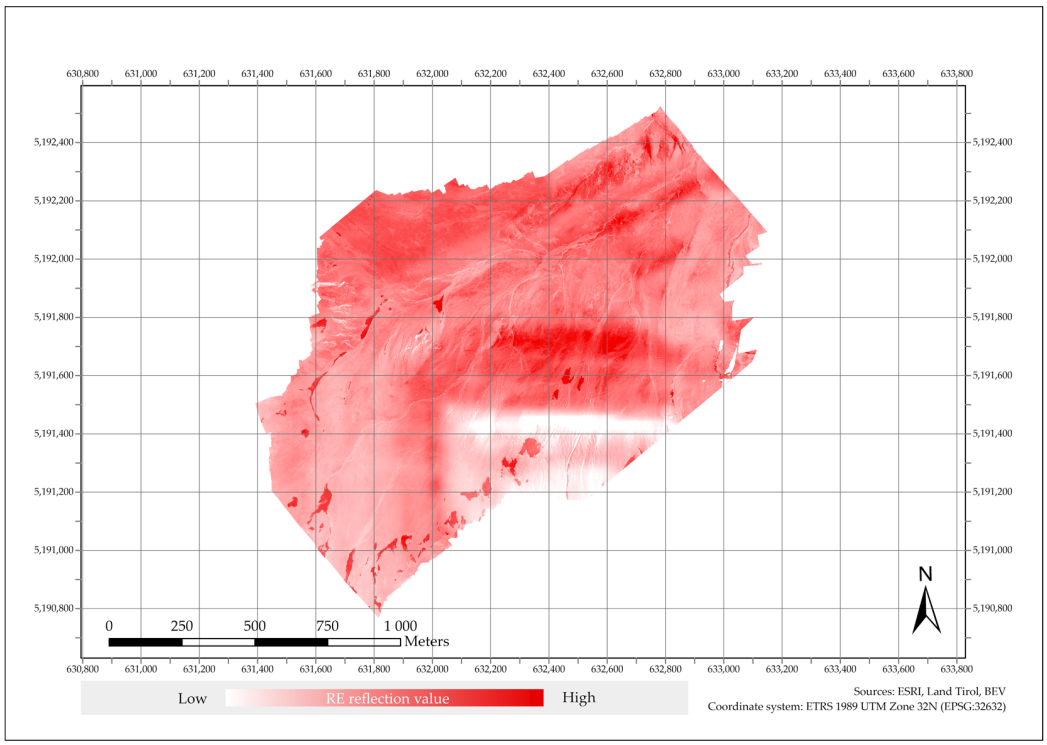

Figure 3. Varying illumination conditions are clearly visible on the RE orthomosaic.

Accuracy Assessment

Initial tests utilizing the CNNs provided accuracy values below 70% and failed several times due to a lack of computational resources, which made a deeper analysis of the obtained results difficult. Simultaneously performed tests with the RF algorithm achieved more promising accuracy values. The best classification results with RF were achieved using the RGB orthomosaic as the foundation of the classification and employing the digital elevation model for additional input data. The DEM was tested against the two available multispectral orthomosaics, the TRI layer and a slope layer, and turned out to be the best supplement for this approach, as presented in Table 3.

Table 3. Supplementary datasets. This table presents the overall accuracy values reached for different supplementary layers when used in combination with the RGB orthomosaic in the classification.

Supplementary Layer	DEM	OCN	TRI	Slope	RE	No Suppl. Layer
Overall accuracy (%)	87.1	73.1	73.0	70.9	69.2	67.0

The classification of the RGB orthomosaic in combination with the DEM achieved an overall accuracy of 87.1%. In the approach where the OCN orthomosaic was used as a supplement, the OA was considerably smaller at 73.1%. When utilizing the TRI layer, the OA was very similar, with 73.0%, while using the slope layer as an additional input resulted in an overall accuracy of 70.9%. The RE orthomosaic was the supplementary dataset that delivered the worst results with less than 70% OA, a performance that was only slightly better than using no additional data with the RGB orthomosaic at all, which resulted in an OA of 67%.

The accuracy of the final classification was assessed by calculating a conventional confusion matrix resulting in the following statistical metrics: overall accuracy (OA), producer's accuracy (PA), user's accuracy (UA) and the Kappa Coefficient. The 659 samples that were not used for training the algorithm were utilized for the validation of the classification results. In 87.1 percent of the samples verified, the classified landcover class matched the actual value, which was determined beforehand by the authors using the RGB orthomosaic. The results of this evaluation are displayed in Table 4, showing the accuracy values of the validation samples from the most accurate classification (RGB + DEM):

Table 4. Accuracy assessment. Confusion matrix displaying the accuracy values of the validation samples for each target class + overall accuracy, producer's accuracy, user's accuracy and Kappa Coefficient for the final classification.

Class Name	Snow	Water	Bedrock	Coarse Sed.	Fine Sed.	Juniper	Thistle	>50% Grass	>50% Forbs and Moss	Total	UA (%)	Kappa
Snow	77	0	1	3	1	0	0	0	0	82	**93.9**	0
Water	0	53	1	13	0	0	1	0	0	68	**77.9**	0
Bedrock	0	0	70	14	0	0	1	0	1	86	**81.4**	0
Coarse sed.	0	8	6	81	0	0	0	1	1	97	**83.5**	0
Fine sed.	1	0	1	3	60	0	0	0	0	65	**92.3**	0
Juniper	0	0	0	0	0	55	4	1	0	60	**91.7**	0
Thistle	0	0	0	2	0	3	69	4	3	81	**85.2**	0
>50% grass	0	0	0	0	0	2	2	51	0	55	**92.7**	0
>50% forbs and moss	0	0	1	2	0	0	2	2	58	65	**89.2**	0
Total	78	61	80	118	61	60	79	59	63	659	0.0	0
PA (%)	**98.7**	**86.9**	**87.5**	**68.6**	**98.4**	**91.7**	**87.3**	**86.4**	**92.1**	**0.0**	**87.1**	0.0
Kappa	0	0	0	0	0	0	0	0	0	0	0.0	**0.854**
OA (%)							**87.1**					

The Kappa value for the best model performance (RGB + DEM) is 0.854. The Kappa coefficient compares the classification results with randomly assigned values for each class. Therefore, one can derive how far a classification result is caused not by chance but by a good model performance. Kappa values of 0.6–0.8 are considered good, and values above

0.8 indicate excellent model performance with very high concordance between the model and the actual ground truth [36].

In simple terms, the producer's accuracy and the user's accuracy describe the accuracy from the point of view of the map producer and the map user, respectively. This means that the producer's accuracy shows how often real features are correctly classified on the final map. User's accuracy, however, shows how often a classified value on the map will actually be present in reality [37]. In the case of class 4 (coarse sediment), the producer's accuracy is the lowest at 68.6%. The RF tool implemented in ArcGIS Pro delivered good results (OA 87.1%) in regard to landcover mapping and vegetation cover.

The final classification results for the whole study area are based on the most accurate RF model, which was trained using the 2686 training samples and validated using the 659 validation samples. The results demonstrate a predominance of non-vegetated areas (>70%), with coarse sediment as the most common class (>30%). Figure 4 shows the geographical distribution of the detected classes, and Table 5 presents the results in absolute and relative values.

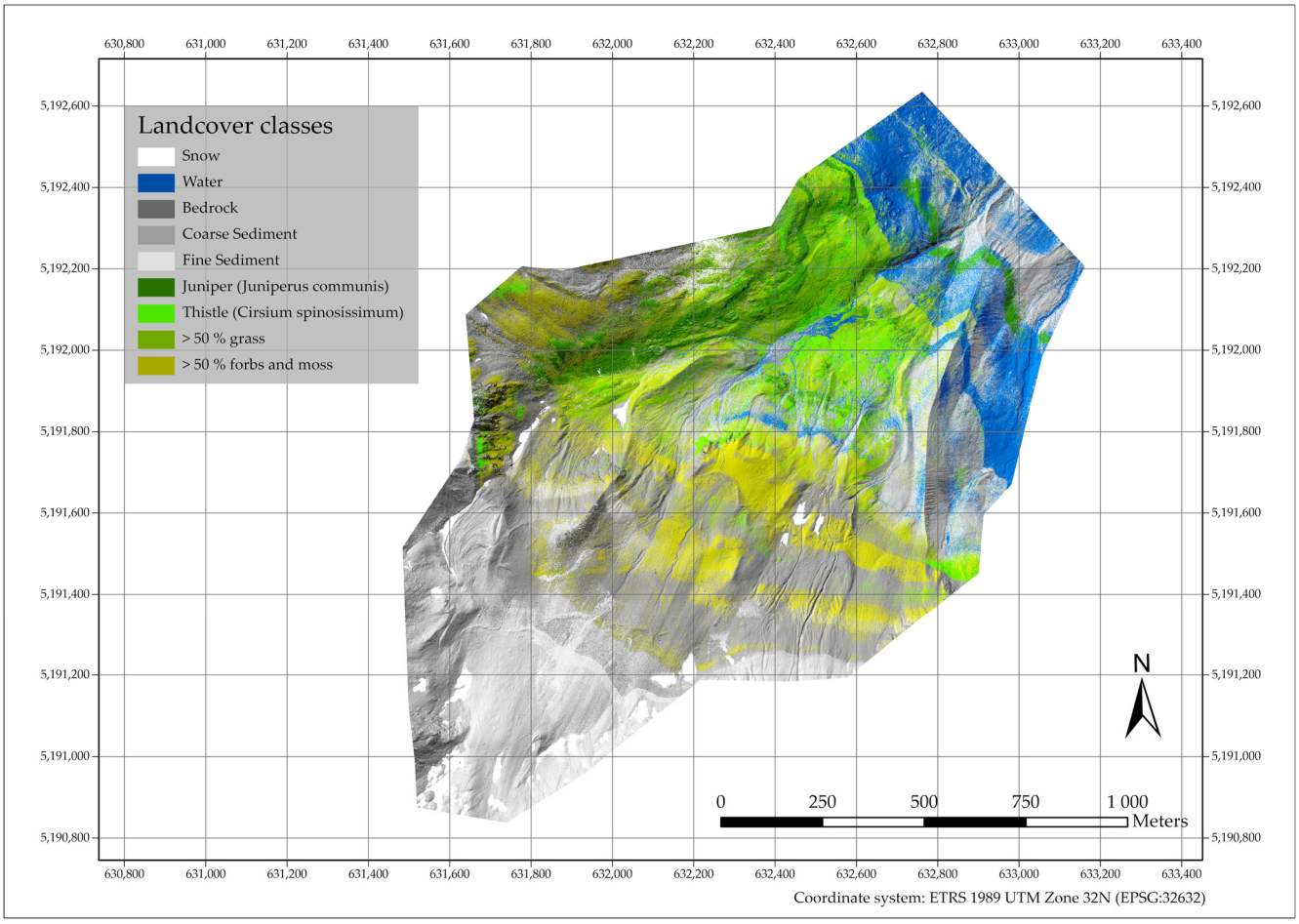

Figure 4. Landcover map of the research area in the Kaunertal Valley.

The most highly evolved species, Juniperus communis, is mostly found in the northern part of the study area in lower regions and, in particular, on south-facing slopes that have been ice-free for at least 100 years. This statement is also true for the grass-dominated mixed-vegetation class. Cirsium spinosissimum often occurs in patches and always in areas with high ground humidity, such as along streams, whereas the mixed vegetation class consisting of >50% forbs and moss is more dispersed and also occurs frequently in higher regions. The highest sections in the southeastern part of the study area are dominated

by large sediment fields and smaller interspersed snow patches, whereby the latter are obviously subject to rapid changes throughout the year.

Table 5. Classification results based on the final RF model. Total and relative distribution of the defined classes in the research area.

Class Name	Total Area (Hectares)	Relative Area (%)
Snow	5.38	3.05
Water	17.96	10.17
Bedrock	41.95	23.76
Coarse sediment	56.99	32.27
Fine sediment	4.47	2.53
Juniper (*Juniperus communis*)	6.26	3.55
Thistle (*Cirsium spinosissimum)*	7.75	4.39
Mixed vegetation with >50% grass	17.53	9.93
Mixed vegetation with >50% forbs and moss	18.29	10.36

Regardless of the terrain age, the most dominant vegetation class is ">50% forbs and moss", except for those regions that have been ice-free for more than 170 years. In this area, the most common vegetation is grass (">50% grass"). In areas that have been unglaciated for at least 100 years (terrain age > 170 years and terrain age < 170 years), the least common vegetation class is "Juniper", whereas, in the two-remaining terrain-age classes, the rarest vegetation form is grass. The youngest terrain in the highest part of the study area has been ice-free for roughly 50 years and is the only sector where not all vegetation classes are present. In this section, no juniper was found at all.

4. Discussion

Using a consumer-grade UAV to perform the surveys in this research turned out to be a sufficient approach as it was able to carry the weight of three small-scale cameras, enabling us to record the area of interest with multiple sensors at the same time. Minor problems regarding flight performance occurred (reduced flight time partly caused by the additional payload and difficulties in stabilizing the aircraft during strong winds) but did not inhibit the planned flights. Given the additional weight on the aircraft and the rough environmental conditions in our research area, these problems might not arise in a different setting such as a lower altitude study area and when using an unmodified UAV. Challenges with stabilizing UAVs, however, are also documented by other authors [38]. To some extent, the limited battery capacity is an issue that still pertains to other settings and restricts the maximum area that can be monitored. If it takes several days to record the whole area of interest (like in our case), there is an increased risk of unstable weather conditions, which might negatively influence the picture quality (e.g., varying illumination conditions and fog on images).

We view the use of low-cost multispectral cameras for classifying vegetation in proglacial areas very critically because the cameras we employed did not deliver satisfactory results for our use case. Illumination problems occurred more severely on the multispectral imagery than on the RGB imagery, even though the intended calibration target was used. Radiometric calibration and atmospheric correction should reduce the adverse effects of varying illumination conditions if performed professionally in a laboratory or at least with a field spectrometer. Such actions improve the measurements of biophysical parameters, as different studies show [39–41]. Employing a superior mount for the multispectral cameras might lead to an improvement because of less blur in the pictures, but the problem of the high sensitivity towards illumination fluctuations still persists.

Due to the large area of interest that needed to be covered by our UAV survey, the creation of multiple flight plans helped to reduce energy consumption and made the flights more efficient. However, we suspect that the arrangement of the flight plans led to

difficulties in the further processing steps. Although we ensured a steady image overlap within the individual flight plans, the overlap between the different flight plans was not always sufficient. We consider this as a possible source of the beforementioned errors that arose in the elevation data during photogrammetric processing. Some artifacts occurred in linear structures in regions where the flight plans adjoined one another. Using the depth maps instead of the dense point cloud for the DEM generation in Agisoft resolved this problem, but the origin of these errors could not be explicitly determined. We assume that the imperfect overlap between the flight plans and patches of fog that moved through the study area while performing the UAV flights created noise in the point cloud that could not be eliminated by filtering.

Manual exposure processing of the original RGB images was omitted in order not to distort the reflectance values, but the brightness differences that were initially present in the RGB orthomosaic could be reduced using the color calibration tool in Agisoft. This increased the quality of the final product but was not enough to completely eliminate the variations. The RGB orthomosaic still turned out to be of high quality and was therefore used as a basis for the classification and for taking the samples, as it is common with ultra-high-resolution datasets [10]. Unfortunately, the multispectral datasets did not reach the desired quality. Negative influences resulting from changing illumination conditions can be observed in the OCN and the RE orthomosaic, as seen in figures two and three, which is why these were excluded from the final classification procedure completely. Although vegetation patterns could be observed by eye, especially on the OCN orthomosaic, the changing light incidence affected the reflection values to such an extent that these datasets eventually became unusable. Excluding the parts of the OCN orthomosaic with the heaviest impairment led to fewer misclassifications but still to a noticeably worse model performance than in the final approach. The RE orthomosaic showed even stronger detriments caused by unstable illumination conditions than the OCN orthomosaic. The TRI and the slope layer were created on the basis of the adjusted DEM and are of high quality. Both datasets were able to increase the classification compared to a run without additional datasets. However, the performance is behind that of the OCN orthomosaic and even more behind that of the DEM (see Table 3). A limitation of the RF algorithm in ArcGIS Pro is the inability to add multiple supplementary datasets to the classification procedure at the same time. This makes determination of the variables which are most suitable for target class discrimination more time-consuming and does not allow a multi-variable classification with more than two layers. However, the performance of training and classification tasks was reliable, as also shown by other authors [42], including a built-in option for accuracy assessment using a confusion matrix.

The vast majority of our research area is unvegetated and covered largely in coarse sediment. The measured distribution of the vegetation in our study area meets our expectations and has a high OA of 87.1%. Accuracy values in the range of 84–93% were also achieved in comparable applications, with single larger species being classified in most cases [10,12,26]. The most highly evolved species in our research area (Juniperus communis) could be detected very well (PA and UA: 91.7%) and was mostly found in lower and sunnier regions. Forbs and mosses formed the most common class and were present in all parts of the research area, whereas thistles (Cirsium spinosissimum) were primarily found in moist areas. The visual resemblance between the three "rock" classes (bedrock, fine sediment, coarse sediment) makes clear demarcations very difficult. This is not only true for the classification algorithm but also for the personnel digitizing the samples. As can be observed in the north and northeastern regions of the study area, a lot of water has been classified. In reality, most of these areas are covered with Juniper. This error results from the beforementioned illumination problems during data acquisition. When flights were performed in this area, the sky was partially covered by clouds which resulted in darker images for this region. Training samples for the water class were also taken from the fringe areas of streams which are characterized by dark-greyish wet sediment. On the produced imagery, these wet rocks appear very much like the Juniper bushes,

which were recorded in shadowed areas because the displayed structures bear a certain resemblance to one another.

One of the biggest challenges in classification tasks is the categorization of present features into target classes. Some kind of generalization based on the corresponding characteristics of these features was needed to meet the demands of a worthwhile classification. This generalization was undertaken by experts in order to represent the given circumstances in a manageable number of classes without losing too much detail on the one hand or overstraining the classification algorithm with overly high demands on the other hand. The maximum accuracy of classification is always limited and hard to predict in advance. This holds true specifically for landcover classifications and vegetation mapping because it is impossible for the researcher to say with certainty which classes will be distinguishable prior to planning the survey. In our case, this complicated the formation of target classes even more. We tried to classify the existent vegetation in as much detail as possible because we knew that we were limited by the resolution of our data anyway. Investigation of the processed imagery revealed that it was only possible to base a distinction on species for the largest plants growing in our research area. Thus, the classes "Juniper (Juniperus communis)" and "Thistle (Cirsium spinosissimum)" are the only classes that actually describe single species, while the remaining vegetation was aggregated into mixed vegetation classes (">50% grass" and ">50% forbs and moss"). The inconsistency of the class formations brought further difficulties because underdeveloped specimens of thistles and junipers might have been included in the mixed vegetation classes as well. A sharp demarcation among the mixed vegetation classes was hard to achieve because the actual size of the plants often fell below the spatial resolution of our imagery. In such cases, the additional use of in-situ samples, as used complementarily in some classification approaches [43], could increase accuracy. The beforementioned fact complicated the creation of training samples for the researchers and lowered the preciseness of the classification. Similar complications occurred with the non-vegetation classes, which were rather coarse. The difficulty of fuzzily defined class borders occurred between the sediment classes (bedrock, coarse sediment, fine sediment), which were impossible to separate definitely because of strong overlaps. Another factor to which attention must be paid is the volatility of the snow class, which changes dramatically during the year and always covers some of the other target classes. With all of these restrictions in mind, one must be aware that a landcover classification always resembles a coarser and temporally fixed reflection of reality. This kind of approach still delivers valuable information on the area of interest and is able to function as the basis for a wide range of further analyses. Accepting a certain degree of uncertainty is always part of the game.

5. Conclusions

We conclude that the use of UAVs in combination with the RF classification algorithm is a suitable approach for detecting sparse vegetation in proglacial areas. Photogrammetrically processed drone imagery provides a sufficient backbone for robust land cover classification. Multispectral data from consumer-grade cameras might offer an added value to vegetation classifications if the quality is sufficient. We found that this kind of imagery is even more sensitive to variations in light than RGB imagery. Therefore, an extended surveying time increases the risk of changing weather conditions which might lead to major problems regarding the recorded reflection values. Severe degradation of the multispectral data forced us to exclude it from the analysis but using only RGB imagery and the DEM in the RF algorithm proved time-efficient and reliable. A limiting factor for UAVs is the battery capacity and, therefore, the maximum size of the study area. Care must be taken as installing additional cameras on a UAV with a low payload impairs the drone's flying behavior significantly, even with an appropriate mount. The combination of the RGB orthomosaic and the DEM produced the best results in our analysis. Other supplementary layers were tested but did not deliver comparable results. Defining target classes for the classification procedure is a crucial step that deserves special attention. The distinction of

said classes might be challenging because of overlaps between the classes and features, which are smaller than the ground sampling distance of the data. In this work, only the largest plants could be distinguished at the species level. All other features were categorized into mixed classes. The implemented RF tool in ArcGIS Pro is a suitable approach for detecting sparse vegetation in alpine areas if a low number of variables are used.

Recommended actions for future research:

- Illumination conditions play a major role in UAV surveys and should therefore be a primary consideration. UAV operators are advised to perform their fieldwork under steady weather conditions and to try to maintain consistent illumination of the study area throughout all flights.
- When dividing the research area into several flight plans, attention must be paid to sufficient image overlap not only within the flight plans but also between them. Linear artifacts in the photogrammetric products may occur in the border regions if this is neglected.
- In cases where battery capacity plays a major role (because of a large study area or additional weight on the aircraft) or when flying under windy conditions, the use of an enterprise-segment UAV with a higher payload and more wind stability is recommended.
- Increasing the spatial resolution of the UAV imagery (by flying at a lower altitude or using a different camera setup) also increases the ground sampling distance of the final orthomosaic, which allows a more precise classification (especially of small features).
- When defining target classes, care should be taken to maintain a sharp distinctiveness of the samples, not only in the field but also on the processed orthoimage. This should lead to fewer misclassifications and reduced fuzziness of the final results.
- For multi-layer classification tasks, we recommend using a different framework than ArcGIS Pro when applying the RF algorithm, one which can include a high number of variables at the same time.

Supplementary Materials: The following supporting information can be downloaded at: https://www.mdpi.com/article/10.3390/rs14194919/s1, Figure S1: DEM with artifacts; Figure S2: Adjusted DEM.

Author Contributions: Conceptualization, U.Z., S.H. and S.K.; Data curation, U.Z. and S.H.; Formal analysis, U.Z., S.H. and S.K.; Funding acquisition, S.K.; Investigation, U.Z. and S.H.; Methodology, U.Z. and S.K.; Project administration, S.K.; Resources, S.H. and S.K.; Software, S.H. and S.K.; Supervision, S.K.; Validation, S.H. and S.K.; Visualization, U.Z.; Writing—original draft, U.Z.; Writing—review and editing, U.Z., S.H. and S.K. All authors have read and agreed to the published version of the manuscript.

Funding: The present study is part of the PHUSICOS (Solutions to reduce risk in mountain landscapes) project, funded by the European taxpayer via the European Union's Horizon 2020 research and innovation program under grant agreement No. 776681.

Data Availability Statement: The data that support the findings of this study are available in the supplementary material of this article or from the corresponding author upon request.

Acknowledgments: We are particularly grateful to Matthias Marbach for his technical support, to Tobias Hanka and Jonas Machold for assistance in the field, to all students and volunteers who supported the fieldwork, to the ENGAGE working group at the University of Vienna for the use of their facilities, and to local stakeholders, namely the agricultural community "Birgalpe" and the operator of the Kaunertal Valley glacier road (Kaunertaler Gletscherbahnen GmbH) for their support and permission to conduct this research.

Conflicts of Interest: The authors declare no conflict of interest.

References

1. Rudolf-Miklau, F.; Hübl, J.; International Research Society Interpraevent. *Alpine Naturkatastrophen: Lawinen, Muren, Felsstürze, Hochwässer*; Stocker: Graz, Austria, 2009.
2. Scheurer, K.; Alewell, C.; Bänninger, D.; Burkhardt-Holm, P. Climate and land-use changes affecting river sediment and brown trout in alpine countries—A review. *Environ. Sci. Pollut. Res.* **2009**, *16*, 232–242. [CrossRef]

3. Erschbamer, B.; Niederfriniger Schlag, R.; Winkler, E. Colonization processes on a central Alpine glacier foreland. *J. Veg. Sci.* **2008**, *19*, 855–862. [CrossRef]
4. Nagl, F.; Erschbamer, B. Kapitel 6. Pflanzliche Sukzessionen im Gletschervorfeld. Vegetation und Besiedlungsstrategien. In *Glaziale und Periglaziale Lebensräume im Raum Obergurgl*; Erschbamer, B., Koch, E.M., Eds.; Innsbruck University Press: Innsbruck, Austria, 2010; pp. 121–142.
5. Matthews, J.A. *The Ecology of Recently-Deglaciated Terrain: A Geoecological Approach to Glacier Forelands*; Cambridge University Press: Cambridge, UK, 1992.
6. Ballantyne, C.K. Paraglacial geomorphology. *Quat. Sci. Rev.* **2002**, *21*, 1935–2017. [CrossRef]
7. Jönsson, P.; Cai, Z.; Melaas, E.; Friedl, M.A.; Eklundh, L. A method for robust estimation of vegetation seasonality from Landsat and Sentinel-2 time series data. *Remote Sens.* **2018**, *10*, 635. [CrossRef]
8. Zeng, Y.; Hao, D.; Huete, A.; Dechant, B.; Berry, J.; Chen, J.M.; Joiner, J.; Frankenberg, C.; Bond-Lamberty, B.; Ryu, Y.; et al. Optical vegetation indices for monitoring terrestrial ecosystems globally. *Nat. Rev. Earth Environ.* **2022**, *3*, 477–493. [CrossRef]
9. Guerini Filho, M.; Kuplich, T.M.; Quadros, F.L.D. Estimating natural grassland biomass by vegetation indices using Sentinel 2 remote sensing data. *Int. J. Remote Sens.* **2020**, *41*, 2861–2876. [CrossRef]
10. Kattenborn, T.; Eichel, J.; Fassnacht, F.E. Convolutional Neural Networks enable efficient, accurate and fine-grained segmentation of plant species and communities from high-resolution UAV imagery. *Sci. Rep.* **2019**, *9*, 17656. [CrossRef]
11. Feng, Q.; Liu, J.; Gong, J. UAV remote sensing for urban vegetation mapping using random forest and texture analysis. *Remote Sens.* **2015**, *7*, 1074–1094. [CrossRef]
12. Sadeghi, S.; Sohrabi, H. Tree species discrimination using RGB vegetation indices derived from UAV images. *UAV Small Unmanned Aer. Syst. Env. Res* **2018**, *1*, 5.
13. Nagendra, H.; Lucas, R.; Honrado, J.P.; Jongman, R.H.; Tarantino, C.; Adamo, M.; Mairota, P. Remote sensing for conservation monitoring: Assessing protected areas, habitat extent, habitat condition, species diversity, and threats. *Ecol. Indic.* **2013**, *33*, 45–59.
14. Nijland, W.; Coops, N.C.; Nielsen, S.E.; Stenhouse, G. Integrating optical satellite data and airborne laser scanning in habitat classification for wildlife management. *Int. J. Appl. Earth Obs. Geoinf.* **2015**, *38*, 242–250. [CrossRef]
15. Kattenborn, T.; Fassnacht, F.E.; Schmidtlein, S. Differentiating plant functional types using reflectance: Which traits make the difference? *Remote Sens. Ecol. Conserv.* **2019**, *5*, 5–19. [CrossRef]
16. Hammer, W. Geologische Spezialkarte der Republik Österreich. In *Blatt Nauders*; Geologische Reichsanstalt: Wien, Austria, 1923.
17. Vehling, L. Gravitative Massenbewegungen an Alpinen Felshängen: Quantitative Bedeutung in der Sedimentkaskade proglazialer Geosysteme (Kaunertal, Tirol). Ph.D. Thesis, Friedrich-Alexander-Universität Erlangen, Nürnberg, Germany, 2016.
18. Efthymiadis, D.; Jones, P.D.; Briffa, K.R.; Böhm, R.; Maugeri, M. Influence of large-scale atmospheric circulation on climate variability in the Greater Alpine Region of Europe. *J. Geophys. Res.* **2007**, *112*, D12104.4. [CrossRef]
19. DJI. Phantom 4 Pro V2.0 Technische Daten. 2021. Available online: https://www.dji.com/at/phantom-4-pro-v2/specs (accessed on 19 December 2021).
20. Curran, P.J.; Dungan, J.L.; Gholz, H.L. Exploring the relationship between reflectance red edge and chlorophyll content in slash pine. *Tree Physiol.* **1990**, *7*, 33–48. [CrossRef]
21. EUMeTrain. Monitoring Vegetation from Space. 2010. Available online: http://www.eumetrain.org/data/3/36/navmenu.php?page=3.2.3 (accessed on 17 December 2021).
22. MAPIR. OCN Filter Improves Results Compared to RGN Filter. 2021. Available online: https://www.mapir.camera/pages/ocn-filter-improves-contrast-compared-to-rgn-filter (accessed on 19 December 2021).
23. MAPIR. Survey3 Camera Datasheet. 2021. Available online: https://drive.google.com/file/d/10gIzOjWVNoG9dvZwmAUG9fVqkEZHXEur/view (accessed on 10 January 2022).
24. Noble, T.; Matthews, N. *Unmanned Aircraft Systems Data Post Processing. Structure from Motion Photogrammetry*; USGS National UAS Project Office: Reston, VA, USA, 2017.
25. Colditz, R.R. An evaluation of different training sample allocation schemes for discrete and continuous land cover classification using decision tree-based algorithms. *Remote Sens.* **2015**, *7*, 9655–9681. [CrossRef]
26. Daryaei, A.; Sohrabi, H.; Atzberger, C.; Immitzer, M. Fine-scale detection of vegetation in semi-arid mountainous areas with focus on riparian landscapes using Sentinel-2 and UAV data. *Comput. Electron. Agric.* **2020**, *177*, 105686. [CrossRef]
27. Haas, J.; Ban, Y. Urban growth and environmental impacts in jing-jin-ji, the yangtze, river delta and the pearl river delta. *Int. J. Appl. Earth Obs. Geoinf.* **2014**, *30*, 42–55. [CrossRef]
28. Van Beijma, S.; Comber, A.; Lamb, A. Random forest classification of salt marsh vegetation habitats using quad-polarimetric airborne SAR, elevation and optical RS data. *Remote Sens. Environ.* **2014**, *149*, 118–129. [CrossRef]
29. Briem, G.J.; Benediktsson, J.A.; Sveinsson, J.R. Multiple classifiers applied to multisource remote sensing data. *IEEE Trans. Geosci. Remote Sens.* **2002**, *40*, 2291–2299. [CrossRef]
30. Miao, X.; Heaton, J.S.; Zheng, S.; Charlet, D.A.; Liu, H. Applying tree-based ensemble algorithms to the classification of ecological zones using multi-temporal multi-source remote-sensing data. *Int. J. Remote Sens.* **2012**, *33*, 1823–1849. [CrossRef]
31. Guan, H.; Li, J.; Chapman, M.; Deng, F.; Ji, Z.; Yang, X. Integration of orthoimagery and lidar data for object-based urban thematic mapping using random forests. *Int. J. Remote Sens.* **2013**, *34*, 5166–5186. [CrossRef]
32. Belgiu, M.; Drăguţ, L. Random forest in remote sensing: A review of applications and future directions. *ISPRS J. Photogramm. Remote Sens.* **2016**, *114*, 24–31. [CrossRef]

33. Topouzelis, K.; Psyllos, A. Oil spill feature selection and classification using decision tree forest on SAR image data. *ISPRS J. Photogramm. Remote Sens.* **2012**, *68*, 135–143. [CrossRef]
34. Du, P.; Samat, A.; Waske, B.; Liu, S.; Li, Z. Random forest and rotation forest for fully polarized SAR image classification using polarimetric and spatial features. *ISPRS J. Photogramm. Remote Sens.* **2015**, *105*, 38–53. [CrossRef]
35. ESRI. An Overview of the Segmentation and Classification Toolset. 2022. Available online: https://pro.arcgis.com/en/pro-app/latest/tool-reference/spatial-analyst/an-overview-of-the-segmentation-and-classification-tools.htm (accessed on 12 January 2022).
36. Liu, K.; Shi, W.; Zhang, H. A fuzzy topology-based maximum likelihood classification. *ISPRS J. Photogramm. Remote Sens.* **2011**, *66*, 103–114. [CrossRef]
37. Humboldt State University. Accuracy Metrics. Introduction to Remote Sensing. 2019. Available online: http://gsp.humboldt.edu/olm_2019/courses/GSP_216_Online/lesson6-2/metrics.html (accessed on 23 January 2022).
38. de Castro, A.I.; Shi, Y.; Maja, J.M.; Peña, J.M. UAVs for vegetation monitoring: Overview and recent scientific contributions. *Remote Sens.* **2021**, *13*, 2139. [CrossRef]
39. Berni JA, J.; Zarco-Tejada, P.J.; Suarez, L.; González-Dugo, V.; Fereres, E. Remote sensing of vegetation from UAV platforms using lightweight multispectral and thermal imaging sensors. *Int. Arch. Photogramm. Remote Sens. Spat. Inform. Sci.* **2009**, *38*, 6.
40. Berni, J.A.; Zarco-Tejada, P.J.; Suárez, L.; Fereres, E. Thermal and narrowband multispectral remote sensing for vegetation monitoring from an unmanned aerial vehicle. *IEEE Trans. Geosci. Remote Sens.* **2009**, *47*, 722–738. [CrossRef]
41. Moriya EA, S.; Imai, N.N.; Tommaselli AM, G.; Miyoshi, G.T. Mapping mosaic virus in sugarcane based on hyperspectral images. *IEEE J. Sel. Top. Appl. Earth Obs. Remote Sens.* **2016**, *10*, 740–748. [CrossRef]
42. Toma, A.; Sandric, I. Mapping Flooded Areas Using Sentinel-1 Radar Satellite Imagery Series through Machine Learning and Deep Learning Methods. In Proceedings of the EGU General Assembly 2022, Vienna, Austria, 23–27 May 2022. [CrossRef]
43. Kattenborn, T.; Leitloff, J.; Schiefer, F.; Hinz, S. Review on Convolutional Neural Networks (CNN) in vegetation remote sensing. *ISPRS J. Photogramm. Remote Sens.* **2021**, *173*, 24–49. [CrossRef]